Sixth International Symposium on Marine Propulsors
smp'19, Rome, Italy, May 2019

Tip Geometry Effects on Performance and Erosion for Tip Rake Propellers

Luis Felipe Sánchez Castro[1], **Heinrich von Zadow**[2], **Florian Vesting**[3]

[1]Knud E. Hansen A/S, Helsingør, Denmark
[2]FRIENDSHIP SYSTEMS AG, Potsdam, Germany
[3]Volupe AB, Gothenburg, Sweden

ABSTRACT

The search for increasing propulsive efficiency of ship propellers leads to the creation of propeller blades with unconventional geometries like Contracted Loaded Tip (CLT) and tip rake propellers. This paper examines the effect of different tip configurations on the performance of the propeller. Such blade geometry deviates, however, from conventional designs at the tip region and can no longer be described with the traditional profile sections transformed onto cylindrical surfaces. Hence, for the variation of tip rake a recently developed method is employed here, which transforms 2D blade sections into 3D space with respect to incoming flow and the local rake. Viscous flow, Reynolds-Averaged Navier-Stokes (RANS) and detached eddy simulation (DES) were used to assess a generic test case. CAESES is used for the fully parametric modeling and shape variation of the KP505 propeller. Variations are created in an automated way and analyzed with RANS simulations in open-water condition during a design exploration study. The results of this exploration phase are used as an input for a number of response surfaces allowing an accurate performance prediction for any variant within the design space. A comprehensive search built upon a nested optimization is carried out based on those surrogate models and provides further valuable insight into the design space. Hereby the thrust is kept at a constant measure for all variants. Two opposing design alternatives are selected to asses their performance in behind ship environment at design and off-design conditions including cavitation prediction erosion risk.

Keywords

Tip rake, Tip load, Fully parametric propeller, Cavitation, Erosion, RANS, DES, Optimization, Surrogate, RSM.

1 INTRODUCTION

Improving propulsive efficiency at design point while obtaining good propeller performance at off-design conditions is a challenging duty during the design process of tip rake propellers. Contracted Loaded Tip (Adalid & Gennaro 2011) and Kappel propellers (Andersen et al 2005) are examples of propellers that improve efficiency.

Given the fact that a propeller must operate at an operational profile encompassing different conditions, it is important that the geometry features of the propeller do not hinder its operation at off-design conditions leading to undesired vibration, high pressure pulses, flow detachment and even worse, propeller blade erosion.

The design approach for new propellers is usually an iterative process where the number of design variants and parameters are kept low in order to cope with the complexity of synthesizing multi-disciplinary requirements and limitations into a cohesive final product that meets the features of a specific ship. Systematic series data, e.g. the well-known B-Series propellers (Van Lammeren et al 1969), can give the designer a solid preliminary design. The fine tuning is then often done by manual variation of a handful alternatives, assessed by lifting line and lifting surface methods and validated with experimental methods. Automated design space exploration and optimization are more and more emerging in the field of propeller design, e.g. Bertetta et al (2012) or Berger et al (2014). However, numerical evaluation of the propeller performance requires computational resources and often takes time, particularly when high fidelity simulations are required to resolve detailed flow characteristics.

The focus of this paper is to study the effects of different tip geometries on the propeller performance. The geometry is modeled in the computer aided design and optimization software CAESES based on a method presented by Praefke et al (2017) which allows flexible modifications of the areas of interest of the blade, i.e. the tip region. Fully parametric modeling allows to generate a Design of Experiments (DOE) with a number of variants that is otherwise difficult to generate and evaluate in a limited design lead time.

To include a simulation driven routine in the early design stage allows to identify the designs that offer enhanced open-water efficiency at the design point and can subsequently be adjusted for off-design condition with short lead times. Such an automated procedure provides the designer with more insight on the interrelation between parameters, constraints and objectives.

This work applies a two-staged design exploration with RANS simulation and a surrogate method with subsequent DES assessment of selected candidates, to account for the complex flow and to limit the computational effort. A pool of design candidates is created in the first stage, evaluating the open-water efficiency with steady state RANS simulations.

In a second stage, thereafter, surrogate models are constructed to further search for promising designs in an enhanced exploitation. Finally, two designs with negative and positive rakes are selected from the secondary exploitation for further analysis at design and off-design condition, where cavitation patterns and Erosion Potential Power (EPP) (Eskilsson & Bensow 2015) are evaluated with URANS-DES method.

In the present work restrictions are set on the design generation and assessment of different tip-rake propellers. The benchmark and baseline design for the parametric propeller model is the KP505 propeller (SIMMAN 2008), whose main characteristics are presented in Table 1. CAESES generates with the parametric model a DOE pool, where the shape of the blade tip is varied through parameters like rake, camber and angle of attack (AOA).

2 MODEL DESCRIPTION

2.1 Flow Solvers

The commercial software Star-CCM+ 13.06.011 was employed for the RANS and DES simulations in this study. Star-CCM+ uses the finite volume method on cell center unstructured mesh. Second order upwind and central difference schemes are used to discretize the convection and diffusion terms. The pressure-velocity coupling is solved with the SIMPLE algorithm. The SST k-ω turbulence model was employed for the steady state open-water simulations.

The DES model was employed for the cavitation simulation, where the Volume of Fluid (VOF) approach is used to track the liquid and vapor interfaces and account for cavitation. The mass-transfer model, employed to evaluate the amount of vapor generated or condensed in the domain, was the Schnerr-Sauer model (Sauer & Schnerr 2000).

2.2 Reference Design

The selected baseline propeller for this work is the KP505, a fixed pitch propeller designed for the KRISO Container Ship (KCS). The main particulars of the KCS are a length between perpendiculars of 230 m and a maximum beam of waterline, depth and draught of 32.2 m, 19.0 m and 10.8 m respectively. The main particulars of the KP505 are summarized in Table 1.

Parameter	units	Symbol	Value
Ship service speed	$[kn]$	V_s	24
Diameter	$[m]$	D	7.9
Scale	$[-]$	λ	31.6
Number of blades	$[-]$	Z	5
Rotation rate	$[RPM]$	n	90.8
Hub diameter	$[m]$	H_D	1.422
Expanded area ratio	$[-]$	A_E/A_0	0.818
Wake fraction	$[-]$	ω	0.275
Shaft depth	$[m]$	T_{shaft}	6.7

Table 1: KP505 particulars.

The 3D blade is created from radial functions of pitch, rake, skew, chord, camber and thickness that can be interpolated based on available discrete data available from SIMMAN (2008). The profile section is a NACA66 with meanline $a = 0.8$. Figure 1 shows the resulting propeller geometry.

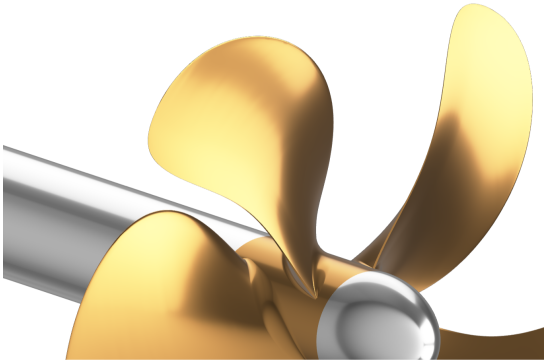

Figure 1: CAD model of baseline propeller from CAESES.

2.3 Parametric Model

In conventional propeller modeling rake is added to the blade by an axial shift of sections on cylindrical surfaces. When following this approach to generate blades with a significant amount of rake the resulting axial shift of sections noticeably limits the design space and also makes it difficult to keep control of the blades shape. Not only does this kind of distortion cause an artificial change in section thickness but it also prevents the proper definition of other profile shape characteristics. These drawbacks become evident when looking at very pronounced shapes such as tip rake propellers. For a blade geometry where the tip points directly in or against axial direction it is impossible to affect the shape via sections that lie on cylindrical surfaces. In such a design the underlying transformations such as pitch and camber are applied in a plane almost perpendicular to the blades span wise direction. As a result, e.g., a change in pitch does not actually raise or lower the leading edge with respect to the incoming flow and a given amount of camber might have only very limited effect. Moreover, any thickness assigned to a certain radial position diminishes down to zero in the above mentioned case.

Hence, the generic modification of an existing propeller geometry towards a design with highly raked tips asks for an adapted modeling technique. Such a technique, along with a detailed explanation on the added value for the designer, has been presented by Praefke et al (2017). The general idea is to transform the 2D sections into 3D space by offsetting them in a local coordinate system that is adjusted both, to the tangent vector of the blades span direction and the local direction of inflow. The resulting sections no longer lie on coaxial, cylindrical surfaces but on arbitrary surfaces depending on the incoming flow, as well as the blades rake given as a function of local radius. A specialty of this approach that allows very intuitive modifications of the design is that the pitch P can be split up into two separate components $P = P_N + P_\alpha$ based on a known

wake field. The nominal pitch P_N hereby represents the component of pitch that shapes the blade such that an angle of attack $\alpha = 0\ ^\circ$ is encountered at any local radius. Consequently, the remaining component P_α describes the pitch due to the actual angle of attack at which each profile section encounters the incoming flow. When applied to conventional propeller designs this technique provides important information about the blade in operation. However, it is also beneficial when it comes to modifying existing propeller geometries towards tip rake designs. By applying the same local angle of attack at any given radius the resulting blade geometry is much more likely to also show performance comparable to the initial variant.

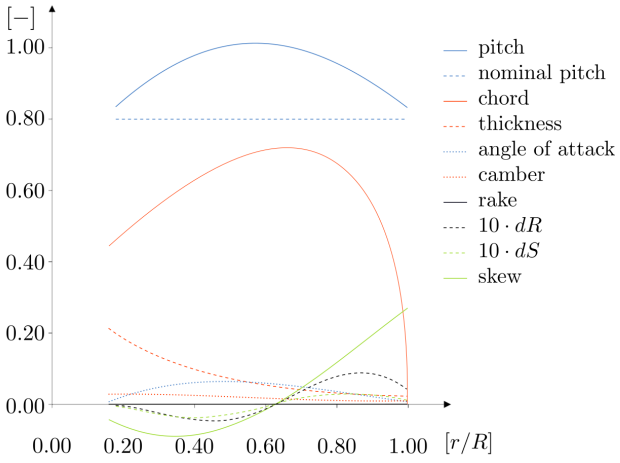

Figure 2: Functions used to control the parametric model.

With the KP505 propeller geometry as a reference design, the first step in creating a tip rake model is to split up the pitch function into the above given measures. An open-water condition with uniform inflow velocity v_a at n revolutions per second is considered. The circumferentially averaged wake velocity $v_w(r) = v_a$ is used to calculate the nominal pitch $P_N = \frac{v_a}{nD}$. Hence, the local angle of attack can be written as

$$\alpha(r) = atan\left(\frac{P(r)}{r\pi D}\right) - atan\left(\frac{P_N}{r\pi D}\right) \qquad (1)$$

based on the given pitch-function. In Figure 2 the resulting functions for the baseline design are shown exemplary at model scale for $v_a = 1\ \frac{m}{s}$ and $n = 5\ s^{-1}$ with the local angle of attack normalized with a factor of $\frac{\pi}{2}$.

When applying pitch to a 2D profile section the center of rotation can be set as the mid-chord position minus a shift dx according to the local skew angle of the blade. If now the angle of rotation is reduced to the fraction originating from the nominal pitch ϕ_N and the local angle of attack α is added as an additional rotation around the mid-chord position of the blade, corrections $dR(r)$ and $dS(r)$ of the rake and skew length, as defined per ITTC (1999) need to be introduced.

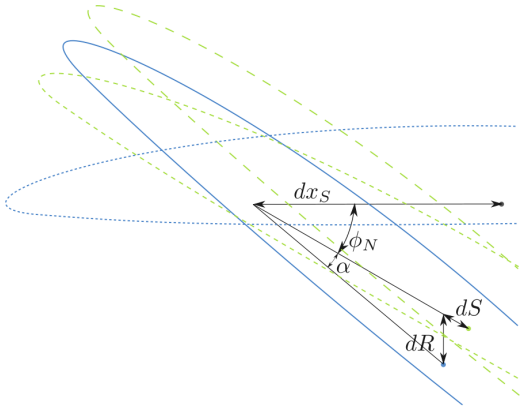

Figure 3: Original profile (fine-dashed) rotated by ϕ_N (medium-dashed) and $\phi = \phi_N + \alpha$ (solid). The coarse-dashed profile originates from the medium-dashed with a local angle of attack α applied around the mid-chord position. Additional rake dR and skew dS needs to be set in order for the coarse-dashed profile to match with the solid one.

This effect of induced skew and rake due to the modified center of rotation is shown in Figure 3 and the resulting offsets can be written as:

$$\begin{aligned} dS &= \frac{dx_S \cdot cos(\phi_N + \alpha) - dx_S \cdot cos(\phi_N)}{cos(\phi_N + \alpha)} \quad \text{and} \\ dR &= dx_S \cdot sin(\phi) - (dx_S - dS) \cdot sin(\phi_N) \quad . \end{aligned} \qquad (2)$$

The functions $dS(r)$ and $dR(r)$ are shown in Figure 2 normalized to the local chord length and scaled by a factor 10 for better visibility. The resulting baseline geometry closely matches the original KP505 with only minor differences due to the offsetting of section data normal to the generator and chord line rather than on exact cylindrical sections. In Figure 4 a color map of the offset in surface - normal direction is given for both geometries with a maximum deviation of 1.2 % of the propeller diameter.

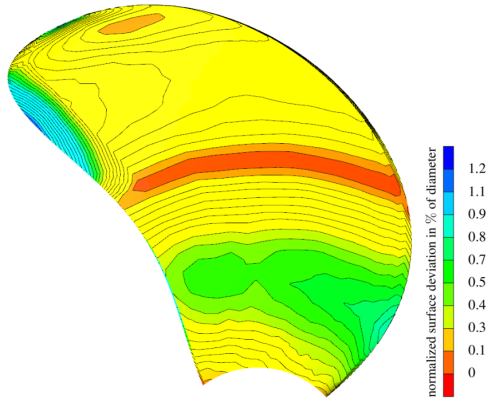

Figure 4: Normal deviation between original KP505 geometry and parametric model normalized with respect to propeller diameter.

Figure 5 shows the variable fillet radius applied at the blade root and also the blunt trailing edge as it has been used throughout this work.

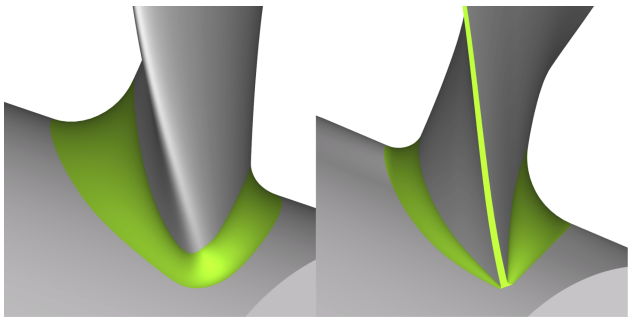

Figure 5: Detailed views of variable fillet and blunt trailing edge.

Design variables are introduced in order to allow a wide variety of shape modifications. A total number of 6 design variables has been used for the initial DOE. The changes in shape are applied to the functions rake, skew and camber. For each function the actual value at the blade tip is introduced as a free variable. A smooth transition towards the original function at lower radii is achieved through the use of B-Spline curves. Additionally the transition range can be modified via another design variable for each of the functions. In Figure 8 the original geometry is shown along with 2 design variants showing how a change in the underlying design variables acts on the shape of the model. The table 2 lists all design variables that have been made available in the model for the form variation. Those design variables with an index $range$ represent the fraction of the relative radius over which the blending is applied from the tip inwards (see Figure 8 for three different sets of resulting design functions).

2.4 Numerical Setup

2.4.1 Domain Setup

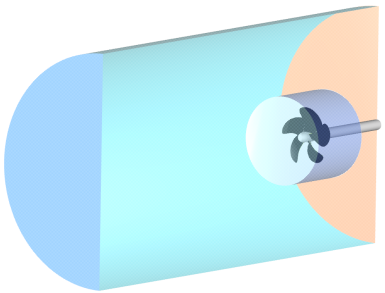

Figure 6: Full computational domain including smaller rotating zone with propeller. Note that domain is trimmed in half only for better visibility.

The computational cylindrical domain can be seen in Figure 6 where the grid interface that separates the rotating and stationary region can be seen.

The domain length applied upstream and downstream from the propeller plane are 2.5 D and 5 D, respectively. The domain radius is 3 D and the shaft extends all the way to the inlet.

2.4.2 Boundary Conditions

The propeller blades and hub are treated as rotating walls. The inlet boundary prescribes a uniform velocity inflow for the open-water simulations and for the behind ship condition it considers the nominal wake field simulated with CFD and measured by Force Technology seen in Figure 7. The outlet boundary condition is defined as a pressure gradient and the outer wall is treated as a slip wall.

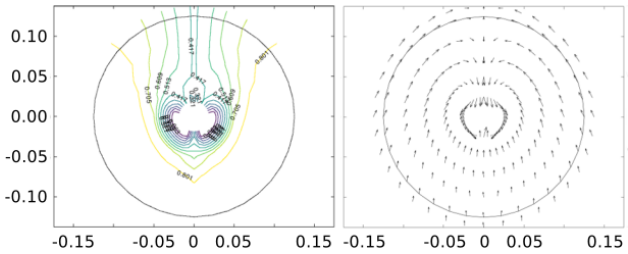

Figure 7: Axial, radial and tangential velocity components of the wake field used to setup the CFD simulations.

The open-water and non-cavitating behind ship condition simulations were carried out in full scale and employed a y^+ in the range $50 < y^+ < 300$ using wall functions. The cavitation simulation employed a y^+ value below 1 ($y^+ < 1$) and was carried out in model scale. Cell count for open-water and behind ship conditions with 1/5 of the domain (1 blade) is 6M cells and for the cavitation simulation 60M cells for the full domain. Fluid properties of water were set as $(\rho_{water}, \mu_{water}) = (1025.88 kgm^{-3}, 1.2187 \times 10^{-3} Pa \cdot s)$ for full scale and $(\rho_{water}, \mu_{water}) = (998.77 kgm^{-3}, 1.0675 \times 10^{-3} Pa \cdot s)$ and for vapor phase $(\rho_{vapor}, \mu_{vapor}) = (0.5953 kgm^{-3}, 1.26765 \times 10^{-5} Pa \cdot s)$ for the cavitation simulation in model scale.

Advanced ratio and cavitation number for this work are defined as $J = V_S \times (1-\omega)/nD$ and $\sigma = 2(p_0 - p_\nu)/(\rho \cdot U_0^2)$, where ω is the wake fraction, n rotation rate $[s^{-1}]$, D propeller diameter, p_0 is reference pressure, p_ν is vapor pressure of water and U_0 is blade tip speed.

The performance of the propeller is evaluated using thrust and torque coefficient and open-water efficiency like:

$$K_T = \frac{T}{\rho n^2 D^4}, \qquad K_Q = \frac{Q}{\rho n^2 D^5}, \qquad \eta_o = \frac{J}{2\pi}\frac{K_T}{K_Q} \quad (3)$$

with T the thrust and Q the torque.

2.5 Optimization Strategy

2.5.1 Exploration

Within CAESES, the initial DOE is carried out based on the 6 free design variables of the parametric model. In this phase of initial sampling, only steady state simulations of the propeller in open-water condition are conducted.

This allows to quickly evaluate a large number of variants which gives a good first insight into the different effects of the changes in shape on the performance of the propeller. A Latin Hypercube Sampling (Helton & Davis 2003) has been chosen to evenly distribute a set of 172 design variants throughout the design space.

2.5.2 Surrogate Enhanced Exploitation

Based on the design space exploration, an accurate surrogate model can be created. The generated Response Surfaces are based on a Kriging (Gao et al 2014) method and allow the prediction of one objective function per generated surrogate model. Separate models are used in parallel to predict both thrust and open-water efficiency at the same time. To asses the prediction correctness, preliminary models are generated based on only half (86) of the available, calculated designs. The prediction of each of the remaining designs is then checked against the calculated CFD result.

The surrogate method shows an averaged accuracy in prediction of η_O of 0.48 % and K_T of 0.765 %, which is in good agreement with the calculated results. The surrogates used for the following enhanced exploitation are based on the entire set of 172 designs. Hence, their prediction can be expected to yield an even higher accuracy.

With the surrogate models available in CAESES, alongside the parametric model, a sophisticated study on the effects of geometrical changes on the propulsive characteristics can now easily be conducted. To ensure that the design variant under consideration can be considered feasible, the generated thrust needs to match that of the baseline design. This matching of thrust is achieved through an inner optimization loop based on a Brent algorithm (Brent 1973). Hereby the local angle of attack in the blade tip area α_{tip} is adjusted such that $K_T = K_{T,baseline}$ for each design variant. If the necessary changes in α_{tip} exceed the range that has actually been investigated with CFD during the initial sampling the design is considered invalid.

3 RESULTS

In total 172 propeller designs are assessed with non-cavitating open-water simulations, varying six design parameters. The performance of 300 more variants has been estimated with surrogate models to find valuable alternatives.

Three subsequent studies have been conducted to search the design space for the most interesting variants. Each study consists of a Sobol sequence of 100 designs, all matching the K_T of the baseline design via the nested optimization as described above. For the first set, different shapes based on the remaining 5 design variables of the parametric model yield a total of 43 valid designs. From another 100 designs that all share the maximum considered amount of tip rake a total of 24 valid designs could be extracted. Finally, another set of designs, this time all featuring the minimum amount of tip rake is studied. This third study did not yield any valid designs as the necessary adjustments in α_{tip} exceeded the initial bounds in all cases. An additional iteration with slightly increased tip rake eventually yields 2 valid design variants with their tip raked towards the incoming flow.

For detailed investigations two designs, one with positive rake and one with negative rake, have been chosen (see Figure 8). While each of the available variants inherently matches the constraint imposed on thrust, their efficiency differs and was therefore considered as a critical measure.

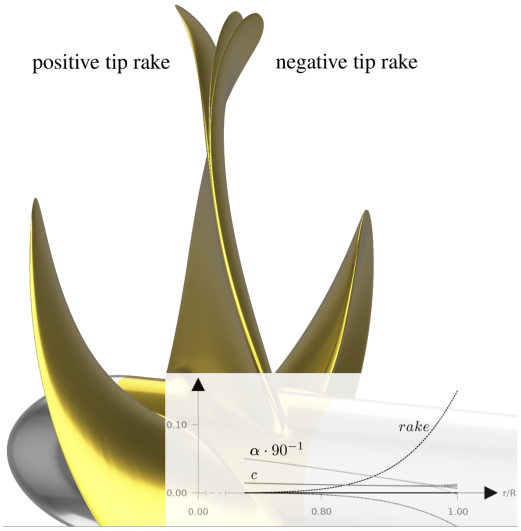

Figure 8: Baseline (KP505) design along with the two selected designs for further investigations.

3.1 CFD verification

In an initial verification phase two different numerical setups have been tested. A model comprising only a rotationally symmetric section of one fifth of the domain has been verified against a similar setup containing the entire 5 bladed propeller. Both models yield the same thrust at the estimated design point of the propeller. The thrust deviation towards the predicted full scale thrust (Holtrop & Mennen 1982 and Holtrop 1984) was within 1.5 %. Due to the shortened simulation times needed the model with one fifth of the domain was chosen to continue the DOE.

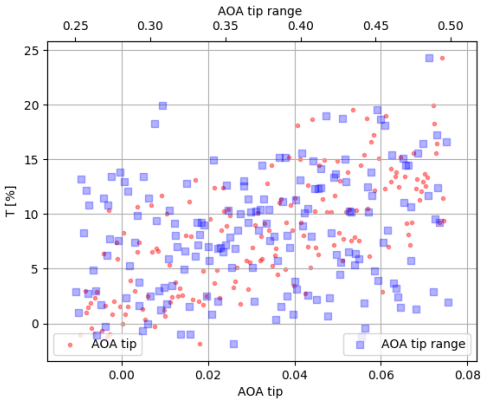

Figure 9: Thrust relative to baseline as function of AOA and AOA tip range.

From the 6 free design variables, the AOA at the tip α_{tip} and the range in which this variable acts α_{range}, were the design variables that played a major role in affecting the measured parameters like thrust and torque, as can be seen from Figure 9-10. Open-water efficiency improvements were marginal, since many of the design samples increased the thrust and torque. During the exploitation no constraints were set to keep the torque of the samples at the same level or below the torque of the baseline design. Including, however, a design variable for the chord distribution could be one option to mitigate the increase in torque, but at the same time it is a design variable that can have positive effects on the pressure distribution along the propeller blade.

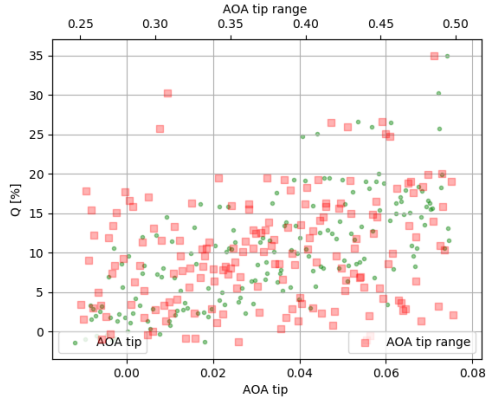

Figure 10: Torque relative to baseline as function of AOA and AOA tip range.

3.2 Analysis of Surrogate Exploitation

The result from this design step is to identify designs with both negative and positive tip rake that generate the same thrust as the baseline design and present good off-design performance. The off-design condition is evaluated for a vessel speed $V_s = 26.2\,kn$ and $N = 112\,rpm$. The designs that fulfilled the evaluation criteria at design and off-design conditions are depicted in Figure 11 and Figure 12.

design variable	lower bound	upper bound	neg. rake design	pos. rake design
α_{tip}	$-0.9\,^\circ$	$6.75\,^\circ$	$-0.870\,^\circ$	$0.014\,^\circ$
α_{range}	0.25	0.5	0.26	0.34
$rake_{tip}$	-0.15	0.15	-0.05	0.15
$rake_{range}$	0.1	0.5	0.47	0.45
c_{tip}	-0.01	0.02	-0.003	0.002
c_{range}	0.1	0.3	0.25	0.28

Table 2: Design Variables and their lower and upper bounds as set for the DOE along with the settings for the two selected candidates.

The design with the negative rake achieves an even distribution of the pressure along the leading edge, which is an early indication of a stable sheet cavitation pattern. The impact of this even distributed loading of the leading edge is reflected in an increment of the thrust by $1.9\,\%$ and torque by $0.6\,\%$ compared to the baseline design. The change in the open-water efficiency is $-0.14\,\%$. Comparing those values to the prediction of the surrogate models shows that the thrust matches with an accuracy of $1.89\,\%$ and the efficiency is predicted to within $-1\,\%$. For the positive rake design the prediction accuracy was found to be slightly higher at $0.3\,\%$ in η_O and $0.84\,\%$.

While searching the design space for variants of interest, the design variables α_{tip} and α_{range} coupled with the tip rake distribution were found to offer good means of improving performance at design and off-design conditions. Hence, fixing the thrust through a nested optimization loop together with the accurate performance predictions available from the surrogate models offers a promising optimization routine in search for increased efficiency.

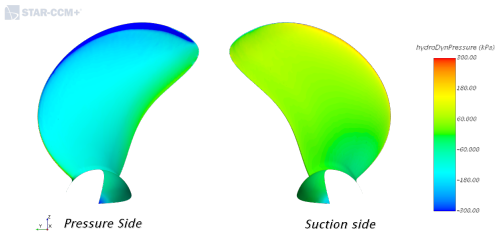

Figure 11: Pressure distribution at off-design condition negative rake design.

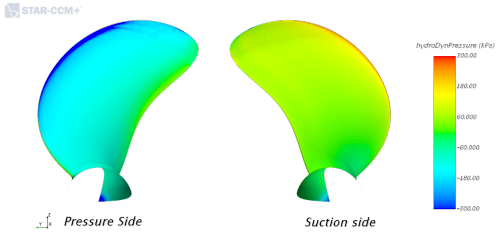

Figure 12: Pressure distribution at off-design condition positive rake design.

3.3 Selected designs for cavitation simulation with CFD

3.3.1 Design condition

The 5-bladed model propeller with a diameter of 0.25 m is used to create the model for the cavitation simulation. The design condition simulated has as input parameters $V_s = 6.1\ m/s$, $N = 24\ rps$, $\sigma_V = 0.20$ and $\sigma_n = 1.91$. Off-design condition has as input $V_s = 4.90\ m/s$, $N = 24\ rps$, $\sigma_V = 0.15$ and $\sigma_n = 1.51$, with $\sigma_V = 2\cdot(p_{stat} - p_\nu)/\rho\,V^2$, $\sigma_n = 2\cdot(p_{stat} - p_\nu)/\rho\,(nD)^2$ and V the tip speed. To assess the risk of erosion, the EPP is calculated as $E_{pot} = V_\nu(p - p_\nu)$, where V_ν is the volume of the microscopic cavity as in Eskilsson & Bensow (2015). The CFD simulations are run with a time step equivalent to $0.5°$ of the rotation of the propeller. The inflow velocity is adjusted to match K_T for design and off-design condition.

The cavitation simulation uses as input for the inlet the wake field presented in Figure 7 and uses the rudder geometry available for the KCS (SIMMAN 2008) as can be seen in Figure 13.

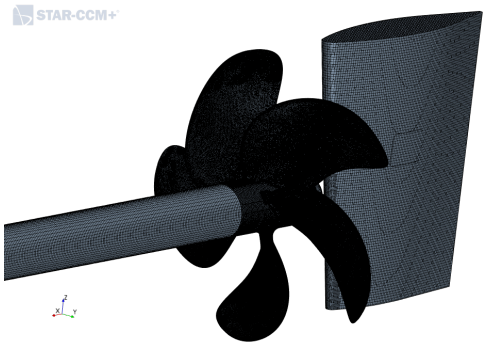

Figure 13: Computational discretization of the domain including the rudder.

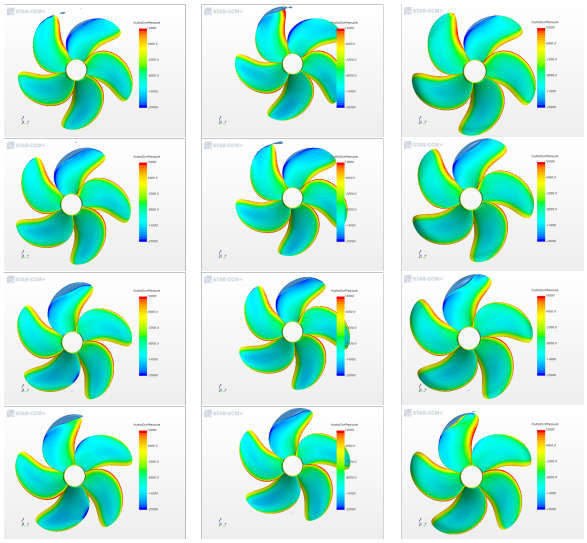

Figure 14: Iso surface of vapor and hydrodynamic pressure distribution on the blade suction side at 4 different blade angles (340°, 350°, 0° and 10° from top to bottom). Left column is baseline design, center column negative rake design, and right column is positive rake design.

In Figure 14 the hydrodynamic pressure $p_H = p + \rho \cdot g \cdot \vec{z}$ distribution is shown on the blade with an iso-surface that corresponds to $5\,\%$ of vapor fraction shown as the cavitation phase. This value is used to have a stable sheet cavitation and to capture detached small cavities. Root cavitation is not observed, and sheet cavitation appears for the baseline design at $0°$ and fades away without detaching suddenly from the blade at $5 - 10°$.

The negative rake design develops sheet cavitation at $0°$ and it is observed until the blade is at $10 - 15°$. For this design it can be seen that the sheet cavitation displays a gradient near the leading edge at approximate $r/R = 0.68$. At the simulated condition this might not be a problem, but as the propeller begins to operate at an off-design condition and the flow accelerates this could generate detachment of sheet cavitation. Variables that could improve the loading in this section of the blade are the AOA, rake and chord (length) distribution.

The positive rake design displays sheet cavitation in the range $0 - 5°$ and the sheet cavitation is smooth without gradients (wavings). This is in line with what could be expected from a positive rake propeller (tip rake points away from the flow) because the region with positive rake is loaded smoothly and the flow is accelerated at a lower rate than the negative rake propeller. This is also observed in the lower thrust that this propeller generates in comparison to both the baseline and negative rake propeller.

3.3.2 Off-design condition

In the off-design condition, the propeller with positive rake presents sheet cavitation that is not fully attached to the leading edge after 5^o. Moreover, the pressure gradients on the suction side along the leading edge also favor the detachment of the sheet cavitation. The detachment of sheet cavitation at 10^o increases the risk of erosion as seen in the graph for the EPP as seen in in Figure 15.

The propeller design with negative rake exhibits a cavitation sheet that develops from $340 - 60^o$. Although the pad of cavitation does detach abruptly from the leading edge, the pressure gradients observed in the graph of the vapor pressure suggest that some detachment at the surface level could take place. Such detachment of sheet cavitation can lead to problems with erosion due to the implotion of cavitation near the trailing edge at approximately $r/R = 0.9$ as seen from the plot of the EPP in Figure 16.

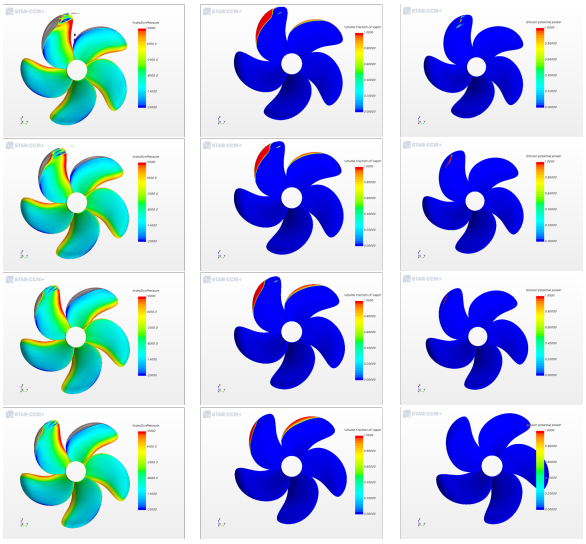

Figure 15: Iso-surface of vapor pressure (left), vapor pressure (middle) and EPP (right) for positive rake design.

4 CONCLUSIONS

A new method to create propellers with different tip geometries is used to model the KP505 propeller and generate different propeller design variations from this baseline. A large DOE pool is used to generate input data for a sur-

rogate model in order to find interesting propeller designs with both positive and negative tip rakes.

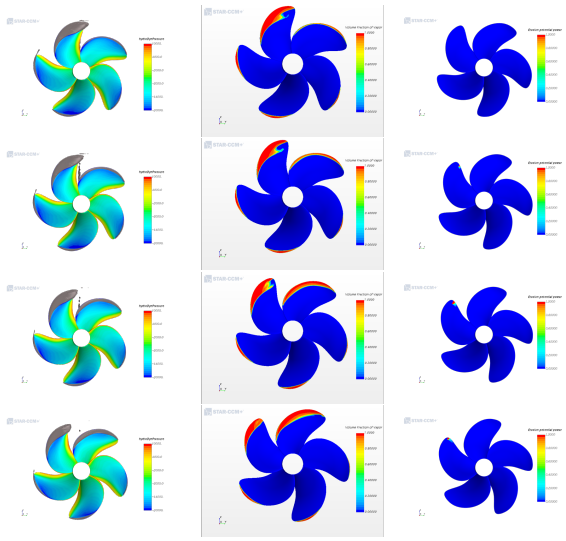

Figure 16: Iso-surface of vapor pressure (left), vapor pressure (middle) and EPP (right) for negative rake design.

It is found that of the six free design variables used in this study, the AOA allowed to control the thrust of the propeller with ease, which allowed to create designs with different tip rake characteristics that did not deviate too much from the target thrust coefficient.

The deviations in thrust and efficiency from the surrogate model and the CFD simulations were in good agreement. This implies that surrogate models could be used in more complex optimization tasks just as well as during design space exploration. However, the surrogate model is more accurate in predicting the characteristics of positive rake propellers than for negative rake propellers. This could be due to the complexity of the physics of the negative rake propellers. Here the flow is accelerated in the tip region and therefore a stronger tip vortex is generated for this propeller compared to the positive rake design.

The designs chosen for further analysis of cavitation with CFD at design and off-design conditions suggest that at design condition both propellers display acceptable vapor pressure gradients although the propeller with positive rake is loaded slightly less than the one with negative rake. At off design condition, the propeller with negative rake develops sheet cavitation in a larger range than the propeller with positive rake. Although the sheet cavitation seems to be uniformly attached to the leading edge, the pressure gradients on the blade and the calculation of erosion power potential suggest that the risk of erosion is higher for the propeller with negative rake.

REFERENCES

Adalid, J. G., Gennaro, G. (2011). 'Latest experiences with Contracted and Loaded Tip (CLT) propellers'. Sustainable Maritime Transportation and Exploitation of Sea Resources, **1**, 47-53.

Andersen, P., Friesch, J., Kappel, J. J., Lundegaard, L., Patience, G. (2005). 'Development of a marine propeller with nonplanar lifting surfaces'. Marine Technology, **42(3)**, 144-158.

Berger, S., Druckenbrod, M., Pergande, M., and Abdel-Maksoud, M. (2014). 'A two-stage optimisation method for full-scale marine propellers working behind a ship'. Ship Technology Research, **61(2)**, 64-79.

Bertetta, D., Brizzolara, S., Gaggero, S., Viviani, M., Savio, L. (2012). 'CPP propeller cavitation and noise optimization at different pitches with panel code and validation by cavitation tunnel measurements'. Ocean engineering, **53**, 177-195.

Brent, R. P. (1973). 'Chapter 4: An Algorithm with Guaranteed Convergence for Finding a Zero of a Function'. Algorithms for Minimization without Derivatives, Englewood Cliffs, NJ: Prentice-Hall.

Eskilsson C. Bensow R. (2015). 'Estimation of Cavitation Erosion Intensity Using CFD: Numerical Comparison of Three Different Methods'. Fourth International Symposium on Marine Propulsors, **SMP'15**, Austin, Texas, USA, June 2015.

Gao D., Ruan N. Xing W. (2014). 'Advances in Global Optimization'. Springer Proceedings in Mathematics & Statistics, 252.

Helton J. C. Davis, F. J. (2003). 'Latin hypercube sampling and the propagation of uncertainty in analyses of complex systems'. Reliability Engineering System Safety, **81**, 23-69.

Holtrop, J. Mennen, G.G.J., (1982) 'An approximate power prediction method', International Shipbuilding Progress **29 (335)**, 166-170

Holtrop, J. (1984). 'A statistical re-analysis of resistance and propulsion data'. Int Shipbuild Prog, **31**, 272-276.

ITTC (1999), 'Model Manufacture, Propeller Models Terminology and Nomenclature for Propeller Geometry', ITTC – Recommended Procedures and Guidelines

Praefke, E., Stoye, T. & Abt, C. (2017). 'A generalized description of hydrodynamic parts based on aerodynamic profile sections', Fifth International Symposium on Marine Propulsors, Espoo, Finland.

Sauer, J., Schnerr, G. H. (2000). 'Unsteady cavitating flow—A new cavitation model based on a modified front capturing method and bubble dynamics' In Proceedings of 2000 ASME Fluid Engineering Summer Conference **251**, pp. 1073-1079).

SIMMAN, 2008, 'Workshop on Verification and Validation of Ship Manoeuvering Simulation Methods', www.simman2008.dk

Van Lammeren, W. P. A., Van Manen, J. D., Oosterveld, M. W. C. (1969). 'The Wageningen B-screw series'. Society of Naval Architects and Marine Engineers **77**(8), p. 43